Sādhanā (2020)45:195
https://doi.org/10.1007/s12046-020-01437-8

Skin friction estimation on a surface under shock-boundary layer interaction

MAITRI KSHETRIMAYUM, KIRAN JOY IRIMPAN and VIREN MENEZES*

Department of Aerospace Engineering, Indian Institute of Technology Bombay, Powai, Mumbai 400076, India
e-mail: viren@aero.iitb.ac.in

MS received 14 March 2020; revised 28 April 2020; accepted 1 July 2020

Abstract. This article presents correlations for indirect measurement of skin friction inside a laminar separation bubble induced by hypersonic shock-boundary layer interaction (SBLI) on a flat plate. The correlations, based on parameters that are known to influence the SBLI region, were developed using exhaustive numerical and analytical studies. Experiments were conducted in a hypersonic shock tunnel at Mach 8.6 (±0.22) to measure surface heat-flux and pressure in the zone of SBLI on a flat plate, which were then used to supplement and validate the correlations. The data predicted by the correlations agreed reasonably well with that of exact solutions. The case studies contained non-reacting air, behaving as a perfect gas on a flat surface.

Keywords. Skin-friction; correlation; hypersonic; SBLI; flow separation; indirect measurement.

1. Introduction

Direct skin friction measurement on hypersonic models is a cumbersome exercise, where the tests have to be conducted in ultra-short-duration test facilities to ensure thermal and ablative survival. The problems often encountered during measurements in short-duration facilities are: (a) underdeveloped boundary layer during millisecond test duration, (b) requirement of pressure, temperature and acceleration compensations on the skin friction sensor, and (c) model vibrations and low sensor output/sensitivity. Despite these difficulties, several researchers attempted development of MEMS [1], fiber optics [2], semi-conductor strain gauge [3, 4] and piezoceramic element-based [5, 6] skin friction sensors. Most of these sensors had a concern of interference from other inputs, such as pressure, temperature and model acceleration. The output of these sensors required extensive calibration and validation to separate the useful measurand from a mixture of interferences, which could induce uncertainty in the measurement. Moreover, a complex flow field, such as the one with hypersonic SBLI, could have enhanced the difficulty level of calibration and compensation for the above sensors. In this backdrop, indirect measurement techniques of skin friction, based on compensation-free sensors and correlations, can be lucrative options of data generation for preliminary design purposes.

Analytically, surface heat-transfer and skin-friction can be linked using Reynolds analogy, which states that the ratio of Stanton number (C_h) and skin friction coefficient (C_f) is a function of Prandtl number (Pr), which is represented by Eq. (1).

$$\frac{C_h}{C_f}(incompressible) = \frac{1}{2}Pr^{-2/3}. \tag{1}$$

Study by van Driest [7] showed that Reynolds analogy, originally derived for incompressible flows (Eq. 1), yields a reasonable approximation for a hypersonic, viscous flow over a flat plate. Later, Goyne *et al* [8] experimentally demonstrated the relevance of Eq. (1) to hypersonic boundary layers, where the Reynolds analogy factor $\left(\frac{2C_h}{C_f}\right)$ predicted by van Driest was found to be consistent with their experimental results. Meritt *et al* [9] observed that Eq. (1) holds good for hypersonic transitional boundary layers on slender, sharp cones. A cone has uniform flow properties along a ray on the surface from the leading edge, which conforms to the zero-pressure gradient condition. They further noticed that the Reynolds analogy is valid for hypersonic flows with pressure gradient, but the Reynolds analogy factor $\left(\frac{2C_h}{C_f}\right)$ does not remain constant in the zone of pressure gradient. Generally, the factor varies between 1.3 and 1.1 for a non-zero pressure gradient at the leading edge of a flat plate in a laminar, hypersonic flow (non-reacting gas), wherein the average value of the factor tends to the one given by Eq. (1) for a Prandtl number of 0.71 for air.

Internal high-speed flows are generally characterized by Shock-Boundary Layer-Interactions (SBLI), where an incident shock on a flat surface generates flow separation and reversal. Such situations are often encountered in

*For correspondence
Published online: 05 August 2020

hypersonic intake flows, where Eq. (1) is not applicable [10]. The Eq. (1) for a compressible case can conceptually be written as a function of viscous hypersonic governing similarity parameters, as in Eq. (2), where, M_e is the Mach number at the edge of the boundary layer of a flat plate, γ is the ratio of specific heats of the gas, and T_w/T_e is the ratio of model wall temperature to the boundary layer edge temperature [11].

$$\frac{C_h}{C_f}(compressible) = f\left(M_e, Pr, \gamma, \frac{T_w}{T_e}\right). \tag{2}$$

The aim of the present investigation is to modify the above equation (2) for region inside the separation bubble by incorporating parameters which are relevant in the study of SBLI. It can be inferred from the study of John and Kulkarni [12] that for SBLI region, inside the separation bubble, $\bar{\chi}$ and $\Delta p/p$ are the relevant parameters. John *et al* [13] has investigated the effect of wall temperature and freestream total temperature on SBLI. The wall temperature affects the temperature distribution within the boundary layer, while the freestream total temperature determines the properties at the edge of the boundary layer, at high speeds. The combined effect of these temperature quantities can be incorporated in the analysis of SBLI by using their ratio T_w/T_0 [13], replacing the ratio T_w/T_e. Therefore, for the separation bubble Eq. (2) can be modified appropriately as,

$$\frac{C_h}{C_f} = f\left(\bar{\chi}, Pr, \gamma, \frac{T_w}{T_0}, \frac{\Delta p}{p}\right), \tag{3}$$

where the viscous interaction parameter ($\bar{\chi}$), which incorporates the effect of Mach number (M_e), is given by,

$$\bar{\chi} = \frac{M_\infty^3}{\sqrt{Re_x}}\sqrt{C^*}, \text{ where } C^* = \frac{\mu_w}{\mu^*}\frac{T^*}{T_w}.$$

From Eq. (3), it is evident that the skin friction can be estimated by heat-flux and pressure measurements at the desired locations on the wall. In practice, direct measurement of skin friction, especially for laminar boundary layers, is difficult due to low SNR (signal-to-noise ratio), which is further low inside the separation bubble. The advantage of indirect measurement of skin friction can be realized by observing Eq. (3), wherein the accurate values of heat-flux (C_h) and pressure, obtained from well-controlled experiments can be used [14]. In the present investigation, simulated results of various SBLI test cases were considered for the study of a laminar separation bubble on a flat plate induced by an incident oblique-shock wave, in order to establish a correlation for indirect measurement of skin friction. Experiments were conducted in a hypersonic shock tunnel to obtain heat-flux and pressure data in the SBLI region, to substitute for the respective parameters in the developed correlation. The indirectly measured skin friction agrees satisfactorily with the results of numerical simulations and experiments.

2. Numerical method and validation

Numerical analysis of the SBLI zone was carried out using *ANSYS fluent 15.0*. A simple wedge-plate model was used for the simulations of SBLI on a flat plate. The cell-centered finite volume discretization method was used to solve the laminar 2-D conservation equations of mass, momentum and energy. The inviscid fluxes were evaluated using an Advection Upstream Splitting Method ($AUSM^+$) scheme, while the diffusive fluxes were central-differenced. The steady solver was used, in which the time marching proceeded until the initial transients were suppressed and a steady-state solution was reached. The temporal discretization followed a linear framework and used an Euler implicit time-marching algorithm combined with a Newton-type linearization of the fluxes. The system of linear equations thus obtained was solved iteratively using ILU method, while an algebraic multi-grid method was employed to accelerate the solution of the coupled sets of equations. *Pressure far-field* boundary condition was applied to the boundaries of the physical domain, whereas, at the outlet, the pressure was extrapolated from the cells inside. The *isothermal wall* boundary condition was applied to the computational model wall. Sutherland's law was used for the viscosity estimation; while a piece-wise polynomial function of temperature was used for the calculation of specific heat at constant pressure.

A wedge-plate model with wedge angle 15°, exposed to the freestream conditions given in case 3 of table 1, was considered to demonstrate a mesh-independent solution, and also to validate the solver with respect to the experimental data of the present study. A structured grid was generated in the computational domain using a grid generating software, *15.0 ANSYS Meshing*. The grid levels were varied through 250×200, 350×300 and 450×400 in the computational domain between the flat plate and wedge for the mesh-independence study. The grid details are given in table 2, whereas a sample grid used in the present study is shown in figure 1. Figure 2 presents the Stanton number (C_h) distribution on the flat plate for different grid levels, demonstrating a mesh independent solution at grid level 350×300. The convergence criterion for the solution was set at a normalized residual value of 1×10^{-6}. The wall pressure and heat-flux (C_h) distribution obtained experimentally in the SBLI zone on the plate is compared with the numerical results in figure 3, where a good agreement between the two data sets is indicated.

3. Experimental methods

The experimental studies were conducted in a hypersonic shock tunnel to measure pressure, Stanton number, freestream and total condition values to be used in the developed correlations. The shock tube of the hypersonic shock

Table 1. Freestream conditions in the shock tunnel for the current experiments.

Case	θ	M_∞	T_w	p_∞	T_∞	T_0
1	10°	8.6±0.22	300*K*	61.9 ± 1.8 *Pa*	41.0 ± 0.8*K*	672.5 ± 8.8*K*
2	12°	8.6±0.22	300*K*	61.3 ± 2.3 *Pa*	40.6 ± 0.6*K*	669.2 ± 11.0*K*
3	15°	8.6±0.22	300*K*	59.4 ± 3.3 *Pa*	40.1 ± 0.9*K*	660.4 ± 15.4*K*

Table 2. Details of the computational grid used for mesh-independence study.

Grid size	$\Delta y_{min}/\delta_0^*$	$\Delta x_{min}/\delta_0^*$ (near LE)	$\Delta x_{min}/\delta_0^*$ (SBLI region)	L_{sb}/δ_0^*
250 × 200	0.009	5.0×10^{-2}	12.1×10^{-2}	23.5
350 × 300	0.006	3.34×10^{-2}	7.74×10^{-2}	23.9
450 × 400	0.003	2.50×10^{-2}	5.63×10^{-2}	24.1

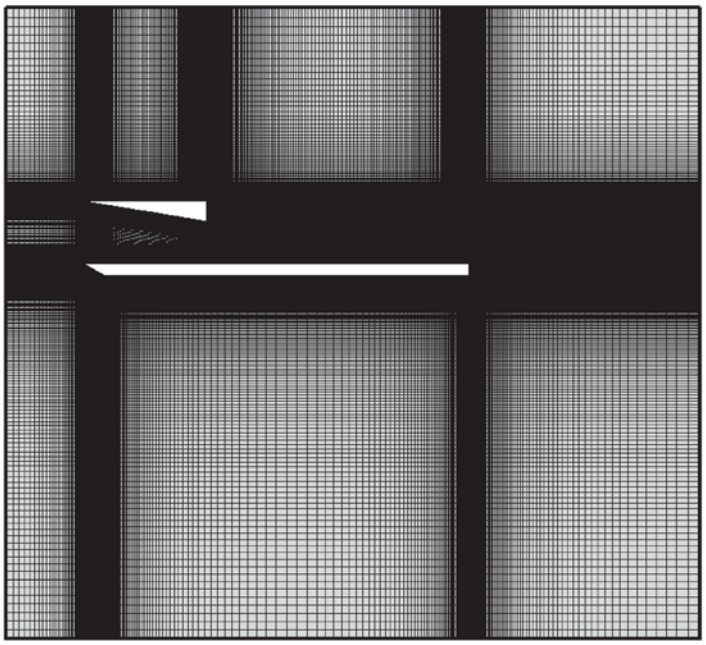

Figure 1. Meshed computational domain used for the numerical study.

tunnel was operated in reflected-shock mode, to generate a heated and pressurized reservoir of air that expanded to a freestream of Mach 8.6 (±0.22) at the test location, through a converging-diverging, conical nozzle of exit diameter 300 mm. A useful test-time of nearly 3 milliseconds was observed in the tunnel in the present study. The test model consisted of a wedge-shaped shock generator, and a flat plate with a width (W) and length (L) of 27cm and 20 cm, respectively. The position and angle of the shock-generator were adjustable to impinge the generated shock at the desired location on the flat plate. A high aspect-ratio ($AR = W/L = 1.35$) was maintained on the flat plate to establish a two-dimensional flow, which was confirmed by pressure readings from locations across the width of the plate (pressure variation in z-direction was less than ±5%). The freestream conditions for the experiments are presented in table 1.

Piezoresistive transducers of Kulite make (XTE-190(M), USA) were used to acquire the transient pressure on the flat plate in the zone of SBLI. The sensors had a sensing junction of 3.8 mm diameter (bead size), a sensitivity range of 2.85-2.93 mV/kPa, a natural frequency and peak operating pressure limit of 150 kHz and 35 kPa, respectively. The pressure sensors were externally excited (at 10 V DC) using a DEWETRON (DEWE 31-32, Austria) signal conditioner.

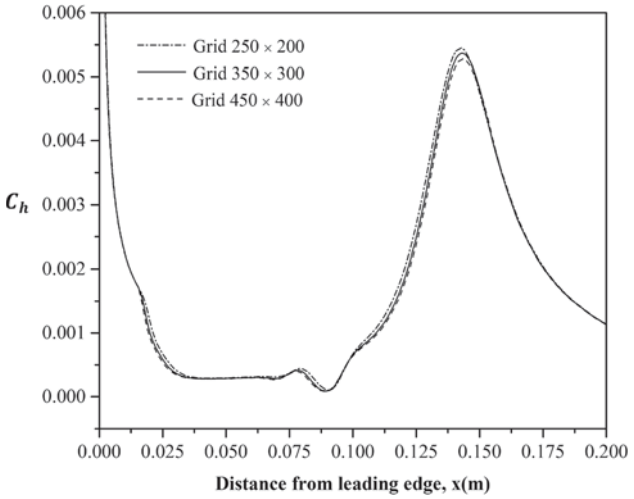

Figure 2. Numerical Stanton number distribution on the flat plate with SBLI, suggesting grid independence of the numerical solution. Flow condition: table 1—case 3.

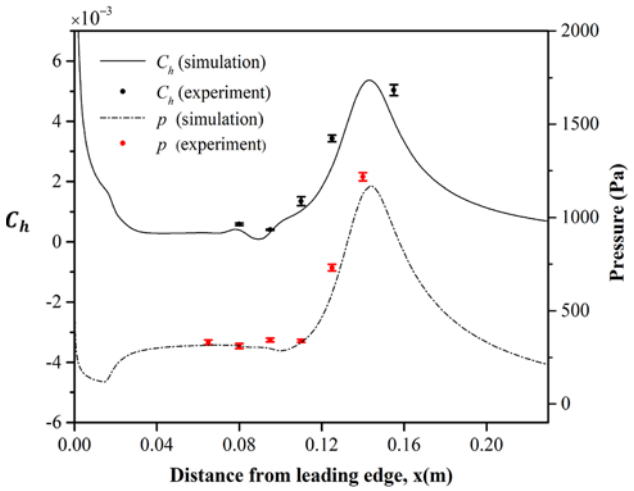

Figure 3. Comparison of simulated and measured Stanton number and pressure distribution on the flat plate with SBLI, presented for code validation. Flow condition: table 1—case 3.

The heat-flux measurements on the flat plate were carried out using Atomic Layer Thermopile (ALTP) sensors (For-Tech HTS GmbH, Germany) [15], with a sensitivity range and peak operating frequency of 79-108 μV/ (W/cm^2) and 300 kHz (response time ≈ 3μs), respectively. The ALTP sensor output was amplified and conditioned using a combination of INA 128 instrumentation amplifiers and DEWE 31-32 signal conditioner. The signals from the sensors were acquired and analyzed using a PC-based data acquisition system equipped with NI PCI-6115 S Series cards.

A standard, 8-inch, Z-type Schlieren system was used for visualization of SBLI on the flat plate. The setup consisted of a continuous light source (150 Watt, xenon-short-arc lamp, UXL-150MO, Abet Technologies, USA) and a high-speed, charge-coupled-device video camera (Phantom V710-1113, Vision Research, USA), equipped with a variable focal length lens of Nikon make (AF Nikkor 80-200 mm F/2.8D ED, Japan). The parabolic mirrors of the Schlieren system had a 64-*inch* focal length. The flow field was visualized at a sampling rate and resolution of 13 kilo-frames-per-second and 800 × 600 pixels, respectively.

4. Correlation and validation

The length of the separation bubble is directly proportional to the wall temperature and inversely proportional to the freestream Mach number and total temperature of the flow. It was observed in the present numerical flow field study that the vortical structure inside the separation bubble depends on the ratio of bubble length (L_{sb}) to displacement thickness (δ_0^*) of the undisturbed boundary layer, where δ_0^* could be estimated using the modified similarity solution for hypersonic boundary layers [16] (refer to nomenclature). The skin friction correlation based on Eq. (3) was developed for two cases, viz. for short bubbles ($L_{sb}/\delta_0^* < 15$) and long bubbles ($L_{sb}/\delta_0^* > 15$), separately. In the case of long separation bubbles, the typical plateau region of the skin friction distribution vanishes, and with further increase in separation, a secondary vortex is formed under the primary vortex, which eventually enlarges and breaks down to form three vortices inside the bubble.

A typical separation bubble formed during SBLI would have two distinct regions on either side of the shock-boundary layer interaction point (I), as shown in figure 4. These regions generally have different pressure, skin friction and streamline distributions owing to varied boundary conditions of the bubble. Inside the separation bubble, except for the small region where the shock interacts with the free-shear layer (figure 4, point 'I'), it was observed through our numerical analyses that for short bubbles, $\frac{C_f}{C_h} \propto \frac{p-p_s}{p}$ and $\frac{C_f}{C_h} \propto \frac{p_r-p}{p}$, for regions 1 and 2, respectively; and for long bubbles, $\frac{C_f}{C_h} \propto \frac{p-p_s}{p}$ and $\frac{C_f}{C_h} \propto \frac{p_r-p}{p_r}$, for regions 1 and 2, respectively, as presented by the plots in figure 5. Therefore, C_f on the wall inside the separation bubble can generally be expressed as Eq. (4), where the linear slope, g (as in figure 5) contains the effects of $\bar{\gamma}_I$ ($\bar{\gamma}$ evaluated at point 'I', which is the point of maximum viscous interaction), T_w/T_0, Pr and γ. In the present study, Prandtl number (Pr) and specific-heat ratio (γ) were assumed to be constant at 0.71 and 1.4, respectively.

$$C_f = g \times C_h \times \frac{\Delta p}{p} \tag{4}$$

The linear slope (g) was determined for regions 1 and 2 using the test cases in table 3 for both short and long bubbles. The coefficient of skin friction at any location $\boldsymbol{x}$ on a wall under SBLI-induced flow separation can then be expressed, based on Eqs. (3) and (4), as:

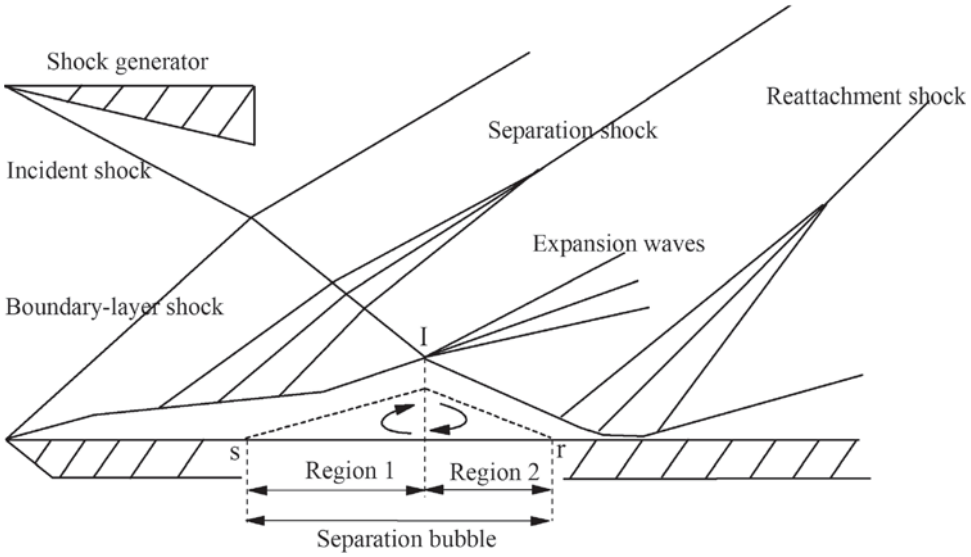

Figure 4. Schematic of incident shock-induced SBLI on a flat plate.

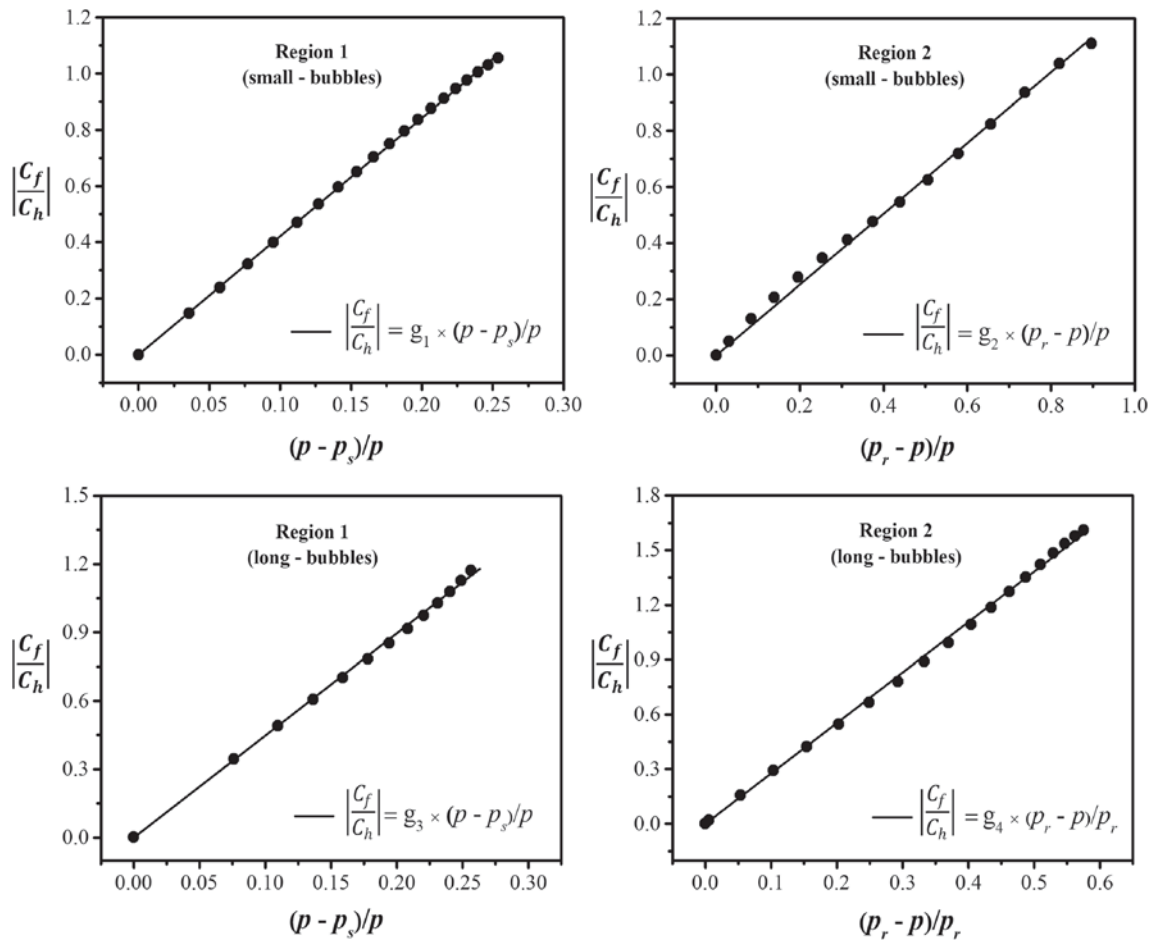

Figure 5. Effect of pressure gradient on wall skin friction in separation bubbles. Plots obtained through exhaustive numerical analyses.

Table 3. Test cases used for the development of correlation.

Case	θ (°)	M_∞	T_0 (K)	T_w (K)	Re (m^{-1})
A	6, 7, 8	10	632, 1000, 1200	200,300,400	2.4×10^6
B	6, 7, 8	8.6	632, 1000, 1200	200,300,400	2.4×10^6
C	6, 7, 8	7	632, 1000, 1200	200,300,400	2.4×10^6

For short bubbles:

$$C_{fx} = g_1 \times C_{hx} \times \left(\frac{p_x - p_s}{p_x}\right) \quad \text{for region 1,} \tag{5a}$$

where, $g_1 = -3.81 \times Pr^{\frac{2}{3}} \times \gamma \times (\bar{\chi}_I)^{-\frac{1}{6}} \times \left(\frac{T_w}{T_0}\right)^{-\frac{1}{20}}$,

and

$$C_{fx} = g_2 \times C_{hx} \times \left(\frac{p_r - p_x}{p_x}\right) \quad \text{for region 2,} \tag{5b}$$

where, $g_2 = -1.88 \times Pr^{\frac{2}{3}} \times \gamma \times (\bar{\chi}_I)^{-\frac{1}{4}} \times \left(\frac{T_w}{T_0}\right)^{\frac{1}{4}}$.

For long bubbles:

$$C_{fx} = g_3 \times C_{hx} \times \left(\frac{p_x - p_s}{p_x}\right) \quad \text{for region 1,} \tag{6a}$$

where, $g_3 = -3.81 \times Pr^{\frac{2}{3}} \times \gamma \times (\bar{\chi}_I)^{-\frac{1}{6}} \times \left(\frac{T_w}{T_0}\right)^{-\frac{1}{20}}$,

and

$$C_{fx} = g_4 \times C_{hx} \times \left(\frac{p_r - p_x}{p_r}\right) \quad \text{for region 2,} \tag{6b}$$

where, $g_4 = -3.27 \times Pr^{\frac{2}{3}} \times \gamma \times (\bar{\chi}_I)^{-\frac{1}{100}} \times \left(\frac{T_w}{T_0}\right)^{\frac{1}{4}}$.

The locations of pressure p_r and p_s (r and s) are as shown in figure 4, whereas p_x is the pressure at any location x along the wall under the separation bubble.

The correlations in Eqs. (5) and (6) can effectively be used by experimental investigators by obtaining the parameters through measurements and analyses. The pressure, Stanton number, freestream, wall and total conditions in the equations can be obtained experimentally by placement of appropriate sensors in the zones of interest. The typical wall heat-flux (C_{hx}) and pressure (p_r, p_x, p_p) traces recorded in the SBLI zone during the current investigation are presented in figure 6, the readings of which are the input to Eqs. (6a) and (6b). The value of L_{sb}/δ_0^* in the current experimental study, for the conditions stated in table 1, was greater than 15 and hence, the separation bubble was classified as a long bubble, as discussed earlier. While p_r and p_x could be measured directly by placing the pressure transducers at the appropriate locations, the measurement of p_s was difficult as the separation zone extended close to the leading edge of the flat plate, making the sensor placement difficult for the measurement. The plateau-

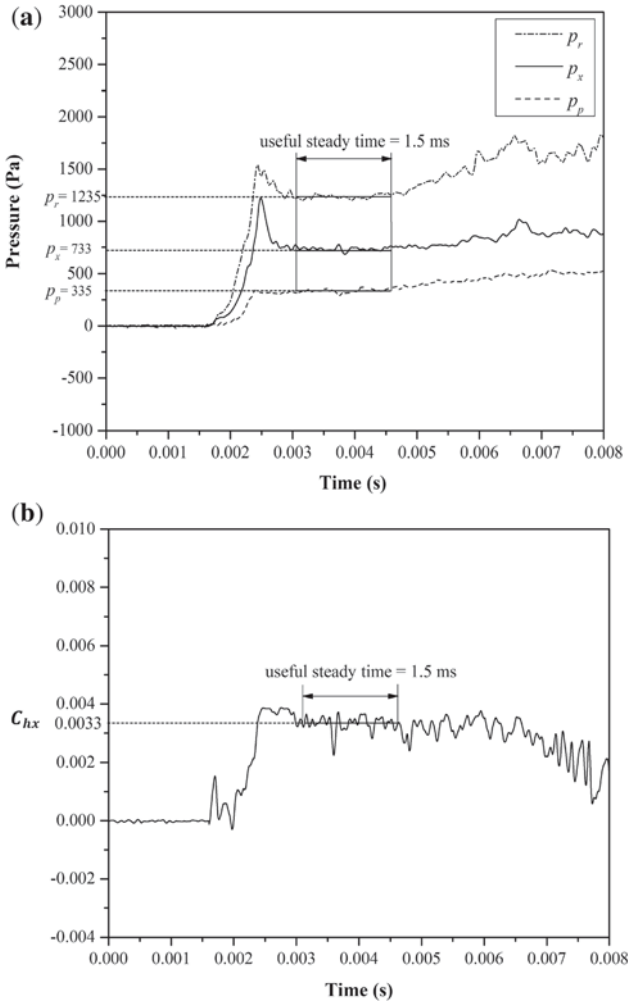

Figure 6. Pressure (a) and ALTP (b) sensors output for θ = 15° (table 1—case 3), C_{hx} and p_x were measured at **x** = 12.5 cm from leading edge of the flat plate.

pressure in the separated zone has been observed varying proportionately as the pressure at the separation point (p_s), as reported by Chapman *et al* [17]. Hence, the value of p_s in Eq. (6a) was taken as = $k \times p_p$, where p_p was the measured plateau pressure (figure 6), and k, the constant of proptionality, was obtained from the numerical case studies. The viscous interaction parameter, $\bar{\chi}_I$ in Eq. (6) was evaluated at location 'I' (figure 4), which was identified experimentally using flow visualization. The other parameters in the expression for $\bar{\chi}_I$ were known from the freestream conditions in the shock tunnel, whereas the model wall temperature, T_w was considered as constant (isothermal wall) at 300 K.

The distribution of coefficient of skin friction on the flat plate in the SBLI zone obtained from Eqs. (6a) and (6b) using numerical and experimental data of g_3, g_4, pressure and C_{hx}, is plotted and compared with the results of numerical simulations in figure 7. The specimen calculations leading to two data points in these plots are presented

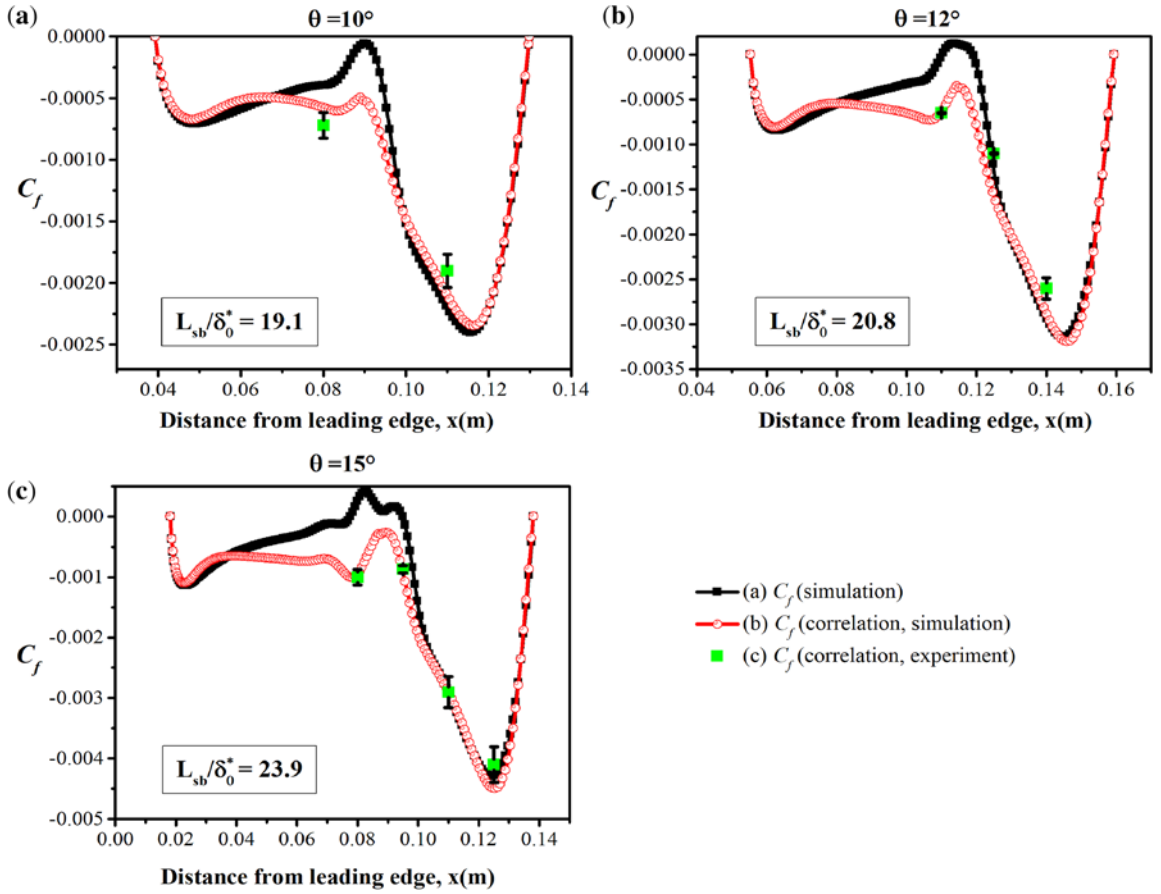

Figure 7. Comparison of coefficient of skin friction distribution for various incident shock strengths on the flat plate obtained through (a) numerical simulations (exact solutions), (b) correlation (Eq. 6) with input parameters derived from numerical simulations, and (c) correlation (Eq. 6) with input parameters derived from experiments.

in table 4. The indirectly measured C_{fx} (correlation with experimental data) agrees reasonably well with the simulated C_{fx} for the cases considered in this study. The deviations in the indirectly measured C_{fx} can mainly be attributed to the error in the measurements of C_{hx}, p_r, p_x, p_p, g_3 and g_4 values. The error estimation in these parameters was carried out based on the method suggested by Coleman and Steele [18], wherein the measurands were assumed to be independent of each other and the errors were governed by the normal/Gaussian distribution. The most probable error in the reported values of indirectly measured C_{fx} was estimated to be less than ±15%. The error is indicated in the form of scatter bars on the plotted data points in figure 7.

The experimental test conditions considered in the present study generated only long separation bubbles in the SBLI zone, and hence, Eqs. (5a) and (5b) could not be validated with the experimental parameters. The numerical validation of these equations is presented in figure 8, where the parameters C_{hx}, p_r, p_x, p_s, g_1 and g_2 were obtained from

Table 4. Measured data as input to Eqs. (6a) and (6b) for specimen calculations.

x (from LE)	θ	C_{hx} (measured) (direct)	p_x (measured) (direct)	p_s (measured) (indirect)	p_r (measured) (direct)	$\bar{\chi}_I$ (measured) (indirect)	T_w/T_0 (measured) (indirect)	$C_{fx_{measured}}$ (indirect)	$C_{fx_{simulated}}$ (direct)
11 cm (Region 2)	10°	1.53E−03	337.57 *Pa*	133.15 *Pa*	578.30 *Pa*	1.40	0.44	−1.9E−03	−2.2E−03
12.5 cm (Region 2)	15°	3.43E−03	730.68 *Pa*	169.51 *Pa*	1217.82 *Pa*	1.40	0.45	−4.1E−03	−4.2E−03

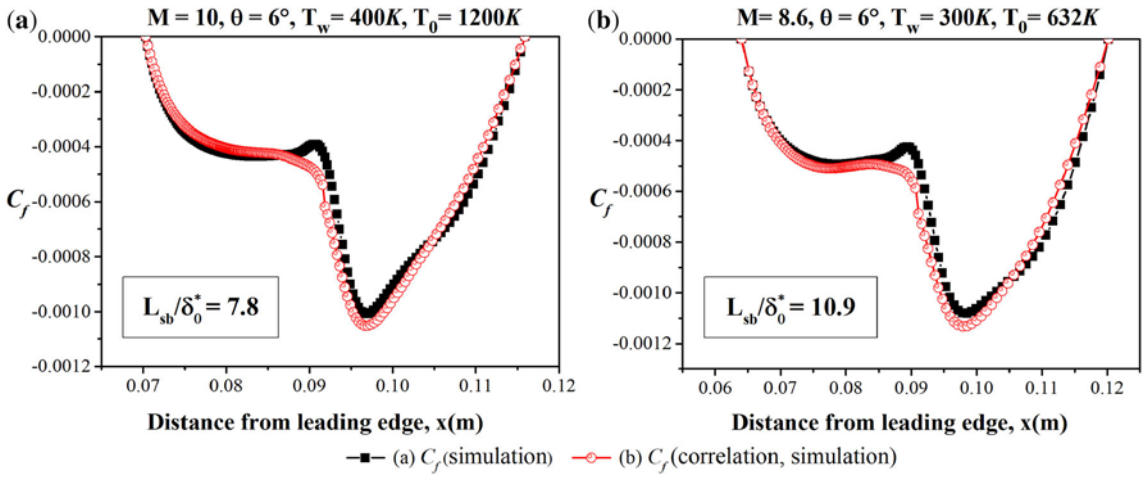

Figure 8. Comparison of coefficient of skin friction distribution on the flat plate for short separation bubbles under SBLI obtained through (a) numerical simulations (exact solutions), and (b) correlation (Eq. 5) with input parameters derived from numerical simulations.

the numerical simulations. The results presented are for the ratio $L_{sb}/\delta_0^* < 15$, which classifies the separation bubble as a short bubble. The plots present a good agreement between the simulated C_{fx} distribution and the one obtained through Eq. (5) using the numerical parameters as stated above.

5. Conclusion

Correlations were developed to estimate skin-friction on a surface under flow separation during hypersonic SBLI. The correlations use surface heat flux, pressure and freestream data of a test over a flat plate to yield skin friction coefficient distribution on a wall under flow separation. The correlations were developed based on a Navier–Stokes solver of *ANSYS fluent 15.0*, and were validated using independent experimental and numerical data. The correlations are applicable to an SBLI at hypersonic Mach numbers, where non-reacting and thermally perfect air is used as a test gas. The development offers an indirect method of skin friction measurement as a function of measured surface heat-flux and pressure on a flat plate during hypersonic SBLI, and can find applications in numerous internal high-speed flows.

Nomenclature

C	Chapman–Rubesin parameter
C_p	pressure coefficient, $2p/(\rho_\infty V_\infty^2)$
c_p	specific heat at constant pressure (J/(kg-K)
C_f	skin friction coefficient, $2\tau/(\rho_\infty V_\infty^2)$
C_h	Stanton number, $q_w/(\rho_\infty V_\infty (h_{ad} - h_w))$
h	enthalpy (J/kg)
h_{ad}	adiabatic-wall enthalpy (J/kg), $h_{ad} = T_0 \times c_p \times \sqrt{Pr} = T_0 \times 1005 \times \sqrt{0.71}$
L_{sb}	length of separation bubble
M	Mach number
p	pressure (N/m^2)
Pr	Prandtl number
q	heat flux (W/m^2)
r	reattachment point
s	separation point
Re	Reynolds number
T	temperature (K)
T^*	reference temperature (K), $T^* = T_\infty\left(1 + 0.032M_\infty^2 + 0.58\left(\frac{T_w}{T_\infty} - 1\right)\right)$
V	velocity (m/s)
x_0	distance from leading edge where shock meets the flat plate in inviscid case
γ	specific heat ratio
δ_0^*	displacement thickness of undisturbed flat-plate boundary layer at x_0, $\delta_0^* = 0.664 \times \frac{\gamma-1}{2} \times \frac{M_\infty^2 x_0}{\sqrt{Re_{x_0}}} \times \left(1 + 2.60\frac{T_w}{T_0}\right)$ for weak viscous interaction
θ	flow turn-angle on the shock generator (wedge angle) (deg.)
μ	coefficient of dynamic viscosity (N-s/m^2)
ρ	density (kg/m^3)
τ	shear stress (N/m^2)
$\bar{\chi}$	viscous interaction parameter
SBLI	shock-boundary layer interaction

Subscripts

e	boundary-layer edge property
I	shock-shear layer interaction point, shown in figure 4
p	pressure-plateau region
r	re-attachment point
s	separation (initiation) point

w wall property
x property at distance 'x' from leading-edge of flat plate
∞ freestream condition
0 total condition
* evaluated at reference temperature, T^*

References

[1] Meloy J, Griffin J, Sells J, Chandrasekharan V, Cattafesta L N and Sheplak M 2011 Experimental verification of a MEMS based skin friction sensor for quantitative wall shear stress measurement. *AIAA Paper 2011-3995*

[2] Vasudevan B 2005 Measurement of skin friction at hypersonic speeds using fiber-optic sensors. *AIAA Paper 2005-3323*

[3] Bowersox R D W, Schetz J A, Chadwick K and Deiwert S 1995 Technique for direct measurement of skin friction in high enthalpy impulsive scramjet flowfields. *AIAA Journal* 33: 1286–1291

[4] Novean M G, Schetz J A and Bowersox R D W 1997 Direct measurements of skin friction in complex supersonic flows. *AIAA Paper 97-0394*

[5] Holden M S 1978 A study of flow separation in regions of shock wave-boundary layer interaction in hypersonic flow. In: *11th Fluid and Plasma Dynamics Conference*, pp. 1169–1190

[6] Kelly G M, Simmons J M and Paull A 1992 Skin-friction gauge for use in hypervelocity impulse facilities. *AIAA Journal* 30: 844–845

[7] van Driest E R 1952 Investigation of laminar boundary layer in compressive fluids using the Crocco method. *NACA Technical Note 2597*

[8] Goyne C P, Stalker R J and Paull A 2003 Skin-friction measurements in high-enthalpy hypersonic boundary layers. *Journal of Fluid Mechanics* 485: 1–32

[9] Meritt R J, Schetz J A, Marineau E C, Lewis D R and Daniel D T 2017 Direct skin friction measurements at Mach 10 in a hypervelocity wind tunnel. *Journal of Spacecraft and Rockets* 54: 871–882

[10] Schülein E 2006 Skin-friction and heat flux measurements in shock/boundary-layer interaction flows. *AIAA Journal* 44: 1732–1741

[11] Anderson J D Jr. 2006 *Hypersonic and High-Temperature Gas Dynamics*. 2nd edn. AIAA, Virginia, pp. 261–374

[12] John B and Kulkarni V 2014 Numerical assessment of correlations for shock wave boundary layer interaction. *Computers and Fluids* 90: 42–50

[13] John B, Kulkarni V N and Natarajan G 2014 Shock wave boundary layer interactions in hypersonic flows. *International Journal of Heat and Mass Transfer* 70: 81–90

[14] Sahoo N, Saravanan S, Jagadeesh G and Reddy K P J 2006 Simultaneous measurement of aerodynamic and heat transfer data for large angle blunt cones in hypersonic shock tunnel. *Sadhana* 31: 557–581

[15] Knauss H, Roediger T, Bountin D A, Smorodsky B V, Maslov A A and Srulijes J 2009 Novel sensor for fast heat-flux measurements. *Journal of Spacecraft and Rockets* 46: 255–265

[16] Moore F K 1961 On local flat-plate similarity in the hypersonic boundary layer. *Journal of the Aerospace Sciences* 28: 753–762

[17] Chapman D R, Kuehn D M and Larson H K 1958 Investigation of separated flows in supersonic and subsonic streams with emphasis on the effect of transition. *NACA Technical Report 1356*

[18] Coleman H W and Steele W G 2009 *Experimentation, Validation and Uncertainty Analysis for Engineers*. 3rd edn. Wiley, New Jersey, pp. 61–81